永磁体磁场对双相高强钢电阻点焊质量的影响

沈 琦, 李永兵, 陈关龙, 林忠钦
(上海交通大学 上海市数字化汽车车身工程重点试验室, 上海 200240)

沈 琦

摘 要: 以 1对中空圆柱形永磁体为磁场源, 系统地分析了外加恒定磁场作用下, 2.25 mm厚热镀锌双相高强钢板 (HDG-DP600)电阻点焊接头的力学性能、熔核尺寸及宏观晶粒组织走向. 试验发现: 在永磁体磁场作用下, 热镀锌双相高强钢点焊接头的拉剪力较无外加磁场情况下提高了 11.01%, 接头的晶粒组织得到一定程度的细化, 熔核形状"长而扁", 熔核直径较无外加磁场情况下增大了 5.20%. 结果表明, 永磁体产生的外部恒定磁场能够有效改善双相高强钢电阻点焊接头性能.

关键词: 永磁体; 双相高强钢; 电阻点焊; 力学性能
中图分类号: TG 453.9 文献标识码: A 文章编号: 0253-360X(2011)04-0021-04

0 序 言

电阻点焊作为一项主要的连接技术广泛应用于轿车车身制造中. 目前, 车身轻量化的发展趋势促使许多先进高强钢材料被引入到车身制造业中. 新材料的应用一方面降低了汽车自重, 另一方面也给电阻点焊技术带来了一系列挑战.

双相钢由于制备时采用特殊的相变强化处理工艺, 在电阻点焊时, 熔化后的高温奥氏体在保压过程中, 奥氏体冷却曲线会穿越其马氏体相变临界区域, 致使双相钢的焊后熔核中形成不同含量和分布的马氏体, 且马氏体组织的方向性较强, 导致熔核区比较脆, 焊点十字抗拉强度及低周疲劳性能都不佳. 使用传统的凿检法进行焊点质量检测时, 容易出现界面断裂.

根据焊接冶金学理论, 细小的等轴晶能够显著提高焊接接头的综合力学性能, 并能明显降低结晶裂纹[1]. 1995年, 吉林工业大学的赵熹华教授[2]通过在铝合金 LY12板材表面涂刷 $K_2TiF_6+KBF_4$盐类混合物作为孕育剂获得了单一的等轴晶组织, 减小了熔核中薄弱面的尺寸, 显著提高了点焊接头的强度; 但该方法受客观条件的限制难以在生产实践中大规模应用. 电磁搅拌技术通过电磁场的非接触作用使高温金属磁流体发生有规律的高速流动, 影响和改变熔化金属的一次结晶过程, 从而达到细化晶粒, 提高其综合力学性能的目的. 由于其附加装置简单、效益高、耗能少, 经过多年的研究发展, 目前已广泛应用于 TIG焊、MIG焊、CO_2激光焊等弧焊工艺[3-4]. 2005年, 哈尔滨工业大学的张忠典教授[5]以普通高强钢 30CrMnSi为研究对象, 分析了永磁体作用下外加磁场对点焊接头质量的影响. 试验证明, 利用外加磁场能够有效改善 30CrMnSi的电阻点焊接头组织. 然而, 针对在车身制造中具有很大实际应用价值的先进高强钢——双相钢的点焊质量磁控技术的研究目前较少; 因此, 作者尝试通过外加永磁体来研究外部磁场作用下的热镀锌双相高强钢的点焊质量问题, 为双相钢电阻点焊质量的磁控技术奠定基础.

1 试验方法

试验对象为热镀锌双相高强钢 HDG-DP600, 其化学成分见表 1. 试件尺寸及搭接长度见图 1.

表 1 HDG-DP600化学成分 (质量分数, %)
Table 1 Chemical composition of HDG-DP600

C	Si	Mn	P	S	Al	Fe
≥0.18	≥0.80	≥2.20	≥0.035	≥0.030	≥0.020	余量

图 2为伺服焊枪点焊系统. 其中, 焊接机器人为日本 FANUC公司的 R-2000iB型六轴机器人, 焊枪为日本 OBARA公司的 AC伺服焊枪. 该伺服焊枪能够精确控制焊接过程, 通过对电极速度、位移

收稿日期: 2009-11-27
基金项目: 国家自然科学基金资助项目 (50705059)

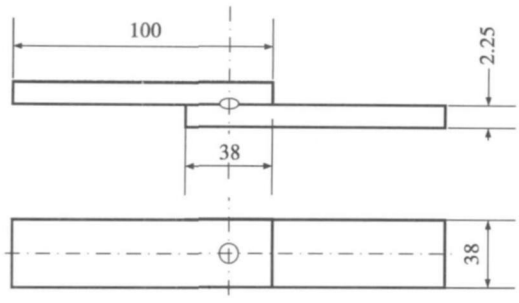

图 1 试件尺寸及搭接长度 (mm)

Fig. 1 Dimension of weldment and overlap joint

的可编程控制,实现对工件的软接触,同时减少对永磁体的振动冲击,确保外加磁场的稳定性和对称性. 焊后的接头质量检测采用深圳凯强利公司 WDW—100电子万能试验机,以及上海光相制样设备公司的金相试验设备.

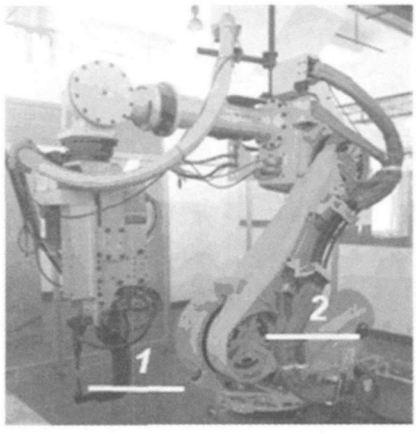

1 – 伺服焊枪 2 – 焊接机器人

图 2 伺服焊枪点焊系统

Fig. 2 Servo gun spot welding system

试验中的外加恒定磁场由 1对中空圆柱形钕铁硼永磁体 BM—N35所产生,其性能参数详见表 2[6].

表 2 BM—N35永磁体性能参数

Table 2 Performance parameters of BM-N35 permanent magnet

剩磁 B_r/T		最大磁能积 B_{max}/(kJ·m^{-3})		矩顽力 b_{Mc}/(kA·m^{-1})		内算矩顽力	工作温度
标准值	最小值	标准值	最小值	标准值	最小值	H_c/(kA·m^{-1})	T/℃
1.21	1.17	279	263	915	860	≥955	≤80

经过加工、装夹后的磁控点焊试验装置如图 3所示. 上、下永磁体 N极相对,永磁体之间产生相斥磁场,以上、下钢板结合面为中心对称面,沿电极臂中心线呈轴对称安装. 图中白色夹具为尼龙绝缘棒,与永磁体过盈配合后通过螺母将其固定. 将永磁体工作距离 W_d定义为上永磁体下端面到上电极端面的垂直距离,或下永磁体上端面到下电极端面的垂直距离. 通过改变工作距离 W_d可以实现对焊接区外加磁场强度的控制,即工作距离 W_d越大,焊接区的外加磁场越弱.

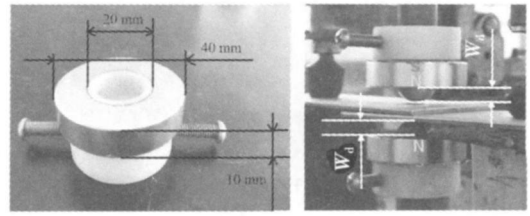

(a) 永磁体 (b) 永磁体安装方式

图 3 磁控点焊试验装置

Fig. 3 Magnetron electromagnetic stirring resistance spot welding equipment

试验中的变量为永磁体工作距离 W_d(图 3),分别取 W_d=6 mm和 W_d=9 mm,以观察外加磁场强度的改变对点焊熔核质量的影响情况. 图 4为电阻点焊过程焊接工艺参数示意图,考虑到材料的镀锌层,将焊接过程分为预热、焊接及回火处理 3段焊形式,从而减弱电极/工件界面铜锌合金化倾向,提高工件/工件的接触电阻,使焊接区加热更均匀[7]. 回火电流则起到部分消除焊接残余应力,提高接头力学性能的作用.

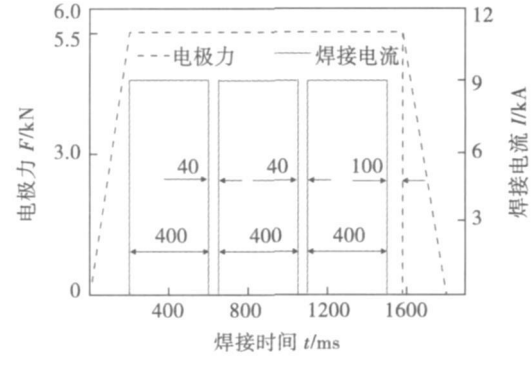

图 4 电阻点焊过程示意图

Fig. 4 Schematic of resistance spot welding process

2 结果和讨论

2.1 永磁体磁场对熔核质量的影响

点焊接头质量的好坏最终反映在强度上,而接

头的强度从宏观上来说则主要取决于熔核尺寸. 在正常的焊接工艺参数条件下(不出现虚焊等情况下),熔核直径与焊点强度近似成正比关系,因而成为反映焊点强度的主要因素,也是汽车工业最常用的点焊接头质量检测方法之一[8]. 图 5为不同外加磁场作用下的点焊接头熔核截面形貌.

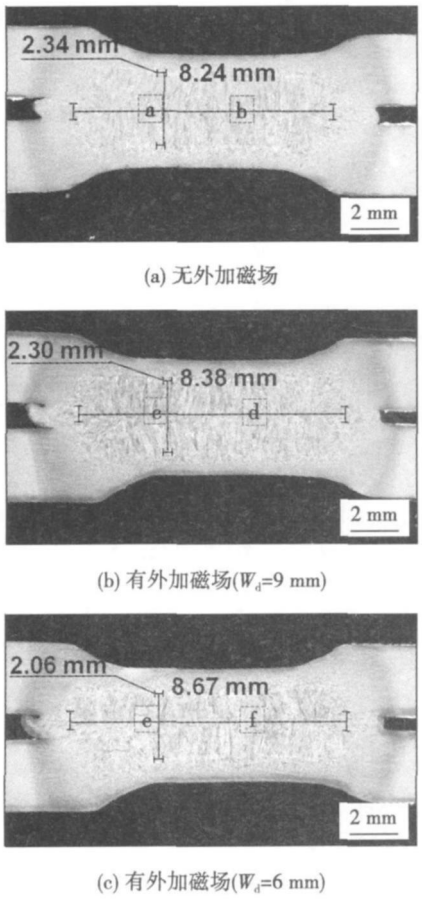

图 5　不同外加磁场作用下的点焊接头熔核截面

Fig. 5　Nugget cross-sections under different external magnetic field

外加磁场作用下获得的点焊熔核"长而扁". 与无外加磁场时的熔核尺寸相比较,当永磁体工作距离 W_d=9 mm时,熔核直径增大了 1.70%;当永磁体工作距离 W_d=6 mm时,熔核直径增大了 5.20%.

图 6为对应于图 5中方框区域的点焊接头熔核截面局部微观组织放大图. 当无外加磁场时,点焊熔核内晶粒组织粗大,枝晶方向性明显,能明显看到工件/工件结合面;有外加磁场时,晶粒组织得到细化,方向性减弱,工件/工件结合面界面模糊.

显然,熔核宏观尺寸以及微观晶粒尺寸的变化是由于磁场的作用引起的. 在电阻点焊过程中,感应磁场引起熔化金属绕着通过电极对称轴的平面内的 4个核心做对称旋转运动,该运动对熔核中的温

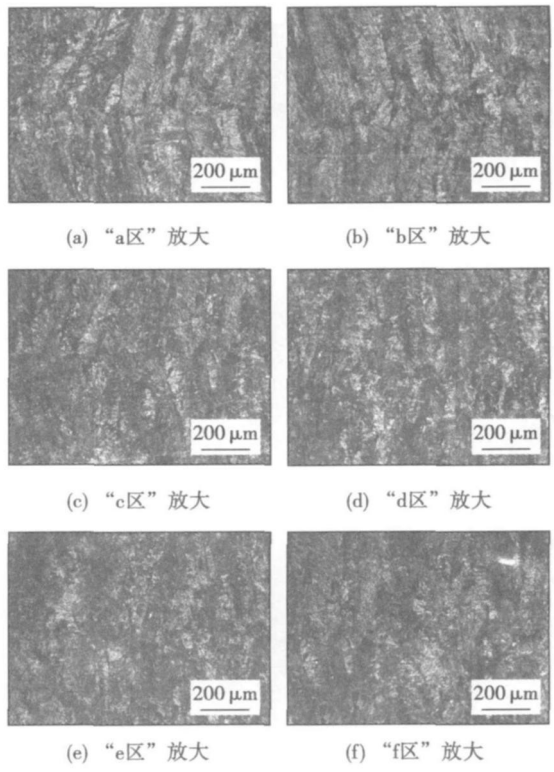

图 6　图 5方框区域晶粒组织放大图

Fig. 6　Partial enlarged details of box region in Fig. 5

度场以及焊核大小都有一定程度的影响[9-10]. 然而,永磁体产生的磁场则垂直于对称面,而且其产生的搅拌力更强烈,迫使液态金属在熔核内做高速离心运动,从而将更多的热量带到边缘,并不断冲刷熔核边缘,因此对晶粒组织和熔核的宏观尺寸产生了较大影响.

2.2　永磁体磁场对点焊接头力学性能的影响

为了检验晶粒细化以及熔核直径的增大对点焊接头力学性能的影响情况,针对永磁体工作距离为 W_d=6 mm, W_d=9 mm及无永磁体这 3种不同外加磁场作用下的接头拉剪力做了比较分析. 每组相同参数做了 6个试件,由于相同焊接条件下的 6个试件的拉剪力值非常接近,其大小在 0.17%以内波动;因此可以认为这组数据较稳定地反映了该焊接条件下的接头力学性能. 拟合同组的 6条曲线,得到图 7所示不同外加磁场作用下点焊接头的拉剪载荷-位移曲线.

从图 7看到,外加磁场作用下的点焊接头强度比无外加磁场时有显著提高,并且接头强度随着永磁体工作距离的减小而增强. 此外,由于电磁搅拌弱化了金属凝固过程的结晶方向性,细化了晶粒组织,因此与常规点焊接头相比,外加磁场作用下的点焊接头塑性均有明显提高. 随着外加磁场的进一步增强,剧烈的搅拌作用加快了熔化金属的冷却

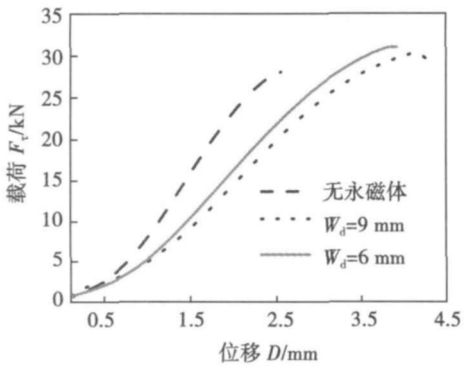

图 7 不同外加磁场作用下点焊接头拉剪载荷—位移曲线

Fig. 7 Tensile-shear load versus displacement curves of spot-weld joint under different external magnetic field

速率，与较弱磁场下的点焊接头相比，较强磁场下的熔核内易形成更多的马氏体组织，因而其接头塑性反而有所下降.

从图 8看到，当永磁体工作距离为 $W_d=9$ mm 时，接头拉剪力较无外加磁场时提高了 8.48%. 随着永磁体工作距离缩短为 $W_d=6$ mm，焊接区的外加磁场强度进一步增强，其拉剪力提高了 11.01%.

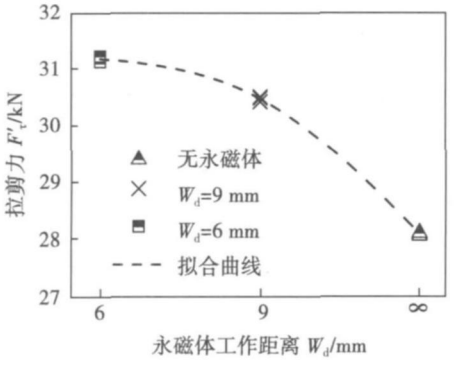

图 8 永磁体工作距离的变化对焊点拉剪力的影响

Fig. 8 Effect of W_d variation on tensile-shear force

3 结 论

通过建立外部磁控点焊试验装置，系统地研究了永磁体磁场作用下的电阻点焊熔核形成过程. 结果表明，永磁体所产生的外部磁场能够有效提高双相钢点焊接头的拉剪力、增大熔核直径、弱化凝固组织的枝晶方向性，因而从整体上提升了双相钢的电阻点焊质量.

参考文献：

[1] 赵熹华，姜以宏. 点焊熔核“柱状＋等轴”组织形成机理分析[J]. 金属科学与工艺，1989，8(3,4)：146—152.
Zhao Xihua, Jiang Yihong. Analysis of the forming mechanism of columnar-equiaxial structure in nuggets[J]. Materials Science and Technology, 1989, 8(3,4): 146—152.

[2] 赵熹华，程亭杰，徐国成，等. 点焊熔核的孕育处理研究[J]. 焊接学报，1996，16(4)：244—247.
Zhao Xihua, Cheng Tingjie, Xu Guocheng, et al. Spot welding nugget incubating process[J]. Transactions of the China Welding Institution, 1996, 16(4): 244—247.

[3] Villafuerte J C, Kerr H W. Electromagnetic stirring and grain refinement in stainless steel GTA welds[J]. Welding Journal, 1990, 69(1): 1—13.

[4] 江淑园，郑晓芳，陈焕明，等. 外加磁场对 CO_2 焊飞溅的控制机理[J]. 焊接学报，2004，25(3)：65—67.
Jiang Shuyuan, Zheng Xiaofang, Chen Huanming, et al. Outside magnetic field control to spatter of CO_2 arc welding[J]. Transactions of the China Welding Institution, 2004, 25(3): 65—67.

[5] 张忠典，王亚荣，李双双. 外加径向恒定磁场改善高强钢点焊质量[C]//第十一次全国焊接会议论文集(第 1册). 北京：机械工业出版社，2005：406—409.

[6] 周寿增，董清飞. 超强永磁体——稀土铁系永磁材料[M]. 北京：冶金工业出版社，1999.

[7] 傅延安，张 红，潘 华. 热镀锌双相高强钢电阻点焊焊点力学性能的研究[J]. 宝钢技术，2005(1)：46—49.
Fu Yanan, Zhang Hong, Pan Hua. Research on mechanical behavior of welding spot of high strength galvanized sheet with dual phase[J]. Baosteel Technology, 2005(1): 46—49.

[8] 赵熹华. 压力焊[M]. 北京：机械工业出版社，1989.

[9] Li Y B, Lin Z Q, Hu Jack S, et al. Numerical analysis of magnetic fluid dynamics behaviors during resistance spot welding[J]. Journal of Applied Physics, 2007, 101(5): 053506-1-053506-10.

[10] Li Y B, Lin Z Q, Hu Jack S, et al. Magnetohydrodynamic behaviors in a resistance spot weld nugget under different welding currents[J]. Science in China Series E, 2008, 51(9): 1507—1515.

作者简介：沈 琦，女，1984年出生，博士研究生. 主要从事电阻点焊质量控制及焊接过程模拟仿真. 发表论文 1篇. Email: Sinkysher@sjtu.edu.cn

通讯作者：李永兵，男，副教授. Email: yongbinglee@sjtu.edu.cn

p. 17—20

Abstract: To overcome the drawbacks of tridiptional structured-light sensor for field-teaching welding robot, off-line programming technique for virtual sensor is introduced. Firstly, the system architecture is designed, then the simulated sensor auto-modeling function is developped, the featured stripe profile for welding object is extracted based on the imaging principle of sensor in virtual scene, and at last actual featured profile recognition by using the programming result is discussed. Experiments on complex weld seam tracking and initial welding point search for strcutured component are executed, and results show the system can enhance the applicability and automation of structured-light sensors in robotic welding.

Key words: simulated sensors; structured-light vision; off-line programming; welding robot

Impact of external magnetic field generated by permanent magnet on quality of dual phase high strength steel by resistance spot welding

SHEN Qi, LI Yongbing, CHEN Guanlong, LIN Zhongqin (Shanghai Key Laboratory of Digital Auto-body Engineering, Shanghai Jiaotong University, Shanghai 200240, China). p. 21—24

Abstract: The joints of hot-dip galvanized dual phase high strength steel (HDG-DP600) thick 2.25 mm were obtained by the resistance spot welding (RSW) process under the external constant magnetic field generated by a pair of hollow cylindrical permanent magnets, and the mechanical property, nugget size and grain structure of weld joints were analyzed. It was found that the tensile-shear force of the joints was increased by 11.01% compared with conventional RSW without the external constant magnetic field, the nugget diameter was increased by 5.20%; the crystal grain was refined and the nugget was wide and flat. The result indicated that the external magnetic field generated by the permanent magnets can effectively improve the quality of the joints of RSW.

Key words: permanent magnet; dual phase high strength steel; resistance spot welding; mechanical property

Effect of Ag content on soldering ability of Sn-Ag-Cu solders

LIU Yang, SUN Fenglian, LIU Yang*, WANG Jiabing (College of Material Science and Engineering, Harbin University of Science and Technology, Harbin 150040, China). p. 25—28

Abstract: The influences of Ag content on melting temperature and wettability of Sn-xAg-0.5Cu (x=0.3, 0.5, 0.7, 0.9) lead-free solder alloys were studied. The melting temperatures of alloys were compared by DSC (differential scanning calorimetry) curves and the wettability was compared by the area and rate of wetting on Cu substrate. The experimental results indicate that alloys with higher Ag content have lower melting points and melting range, and the content of Ag in solder alloys has a significant impact on the distribution and profile of the DSC curves. However, with the Ag content increasing, the wettability of the alloys degrades. By combining the two key properties of solder alloy, melting temperature and wettability, Sn-0.7Ag-0.5Cu shows higher performance.

Key words: lead-free solder; melting temperature; wettability

Analysis of stress corrosion cracking behavior of B101 coiled tubing

BI Zongyue*, ZHANG Kun, LEI Ali, FENG Lajun (1. School of Materials Science and Engineering, Xi'an University of Technology, Xi'an 710048, China; 2. Baoji Petroleum Steel Pipe Company Limited, Baoji 721008, China). p. 29—32

Abstract: The behavior of H_2S stress corrosion cracking of coiled tubing was investigated, the fracture morphology was observed by scanning electron microscope, and the elemental composition of fracture was analyzed by energy disperse spectroscopy. The fracture mechanism was analyzed from the aspects of environment factor, material structure and chemical constitution. The results show that the base metal is insensitive to stress corrosion, and the weld is the weak region of stress corrosion. The weld fracture can be subdivided into four periods: crack incubation period, crack development period, crack rapid growth period with a smoother fractured surface and eventual failure period. The effect of stress change on sulfide stress corrosion cracking is relatively less in the yield strength of 72%—90%. The weld defect, segregation and inclusion are the main factors that make the coiled tubing have low resistance to hydrogen sulfide corrosion.

Key words: coiled tubing; H_2S; stress corrosion cracking

Technique of nickel-based alloy coating produced by hand electric-spark depositing process

ZHANG Ping, MA Lin*, LIANG Zhijie, ZHANG Erjiang (1. Science and Technology Laboratory on Remanufacturing, Academy of Armored Force Engineering, Beijing 100072, China; 2. Office of Compliance Affair, Institute of Chemical Defense, Beijing 102205, China). p. 33—36

Abstract: Because the surface properties of tool steel can be improved through nickel-base alloy coatings achieved by electric-spark deposition technology, the nickel-based strengthen alloy coating on the surface of steel 45 is achieved by the hand electric-spark deposition equipment. The effects of the processing parameters such as thickness, hardness and microdefect on the coatings are analyzed. Through some tests, the parameters are optimized and the coating with better properties is obtained. The study indicates that the coating with best combination property, which thickness is about 595 μm, microhardness is 362 HV and there are no apparent defects in the coating, is produced when the output voltage is 128 V, the output power is 1.2 kW, and the argon atmosphere is 5 L/min.

Key words: electric-spark deposition; nickel-based alloy; depositing technique

Comparative analysis for joint performance of duplex stainless steel by different arc welding methods

WANG Zhiyu, HAN Jian, SONG Hongmei, JIANG Laizhu, WU Weiwei, ZHANG Wei (Research and Development Center, Baoshan Iron & Steel Co., Ltd., Shanghai 201900, China). p. 37—40

Abstract: The welding tests are conducted on 15 mm thick plates of duplex stainless steel 2205 by three different arc